Centroidal Voronoi Tesselation of Line Segments and Graphs

Lin Lu, Bruno Lévy, Wenping Wang

Centroidal Voronoi Tesselation of Line Segments and Graphs

Lin Lu Bruno Lévy Wenping Wang

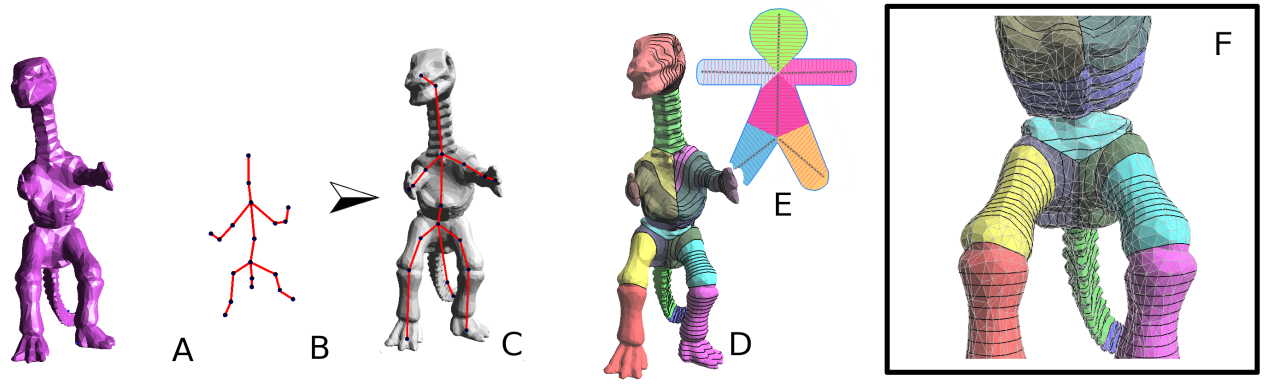

Figure 1: Starting from a mesh (A) and a template skeleton (B), our method fits the skeleton to the mesh (C) and outputs a segmentation (D). Our main contribution is an extension of Centroidal Voronoi Tesselation to line segments, using approximated Voronoi Diagrams of segments (E). Segment Voronoi cells (colors) are approximated by the union of sampled point's Voronoi cells (thin lines, right half of D). Clipped 3D Voronoi cells are accurately computed, at a sub-facet precision (F).

Abstract

Centroidal Voronoi Tesselation (CVT) of points has many applications in geometry processing, including re-meshing and segmentation to name but a few. In this paper, we propose a new extension of CVT, generalized to graphs. Given a graph and a 3D polygonal surface, our method optimizes the placement of the vertices of the graph in such a way that the graph segments best approximate the shape of the surface. We formulate the computation of CVT for graphs as a continuous variational problem, and present a simple approximated method to solve this problem. Our method is robust in the sense that it is independent of degeneracies in the input mesh, such as skinny triangles, T-junctions, small gaps or multiple connected components. We present some applications, to skeleton fitting and to shape segmentation.

CR Categories: I.3.5 [Computer Graphics]: Computational Geometry and Object Modeling—Geometric algorithms, languages, and systems; Algorithms

Keywords: geometry processing, centroidal voronoi tessellation, geometric optimization, Lloyd relaxation, triangular meshes, numerical geometry

1 Introduction

In this paper, we propose a generalization of Centroidal Voronoi Tessellation (CVT). CVT is a fundamental notion that has a wide spectrum of applications in computational science and engineering, including geometry processing. Intuitively, CVT optimizes the placement of points in a domain (for instance the interior of a 3D surface), in such a way that the set of points evenly samples the domain. In this paper, our goal is to show that the main idea of CVT can be generalized to more complicated settings. Namely, we show that an existing set of possibly interconnected segments can be optimized to obtain the best fitting to the interior of a surface. Our generalization of CVT is obtained by using the variational characterization (minimizer of Lloyd's energy), adapted to line segments. To optimize the objective function, we propose a new algorithm, based on an approximation of Voronoi diagrams for line segments and an efficient yet accurate clipping algorithm.

As an application of the method, we show how a template skeleton can be fitted to a mesh model. Our method is simple, automatic, and requires only one parameter (regularization weight). We also show examples of mesh segmentations computed by our method.

Our contributions are:

- A generalization of Centroidal Voronoi Tesselations for line segments, based on a variational characterization. Our formalization can take structural constraints into account, such as a graph of interconnected segments that share vertices;
- an efficient 3D polygon clipping method, that computes the exact mass and barycenter of the clipped Voronoi cells;
- based on this clipping algorithm, a method to compute the CVT of line segments and graphs in 3D, that is both simple (see algorithm outline page 4) and robust to most degeneracies encountered in 3D meshes (cracks, T-junctions, degenerate triangles ...);
- a segmentation method that does not depend on the initial discretization. Part boundaries can pass through triangles, and parts may group several connected components (e.g. trousers with the legs, hair with the head ...);
- *Limitations:* Our method needs a correct orientation of the facets (i.e., coherent normals). Our skeleton-fitting application may fail on some shapes, for instance when the arms are too close to the body (some failure cases are shown).

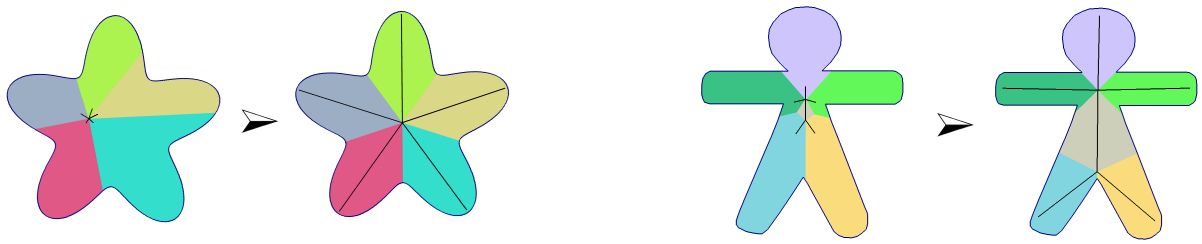

Figure 2: Principle of our method: two examples of Centroidal Voronoi Tesselations for connected line segments in $2D$.

2 Previous Work

Centroidal Voronoi Tesselation

CVT for points A complete survey about CVT is beyond the scope of this paper. The reader is referred to the survey in [Du et al. 1999]. We will consider here the context of Geometry Processing, where CVT was successfully applied to various problems. Alliez *et al.* developed methods for surface remeshing [2002], surface approximation [2004] and volumetric meshing [2005]. Valette *et al.* [2004; 2008] developed discrete approximations of CVT on mesh surfaces and applications to surface remeshing. In all these works, the nice mathematical formulation of CVT resulted in elegant algorithms that are both simple and efficient. However, they use some approximations, that make them dependent on the quality of the initial mesh. For instance, applications of these methods to mesh segmentation are constrained to follow the initial edges, and applications to 3D meshing need to approximate the clipped Voronoi cells using quadrature samples.

Recently, the computation of CVT was fully characterized as a smooth variational problem, and solved with a quasi-Newton method [Liu et al. 2008]. In this paper, we use the smooth variational approach, and replace the approximations used in previous works with an accurate computation of the clipped 3D Voronoi cells, thus making our algorithm independent of the initial discretization.

CVT for line segments A first attempt to compute segment CVT was made in 2D, in the domain of Non-Photorealistic Rendering [Hiller et al. 2003]. The approach is based on a heuristic, that is difficult to generalize in 3D, and that cannot be applied to graphs (more on this below). In contrast, we propose a variational characterization of CVT together with a general algorithm to solve the variational problem.

Skeleton Extraction

Numerous methods have been proposed to extract the skeleton of a 3D shape. We refer the reader to the survey [Cornea and Min 2007]. Based on the underlying representation, they can be classified into two main families :

Discrete volumetric methods resample the interior of the surface, using for instance voxel grids [Ju et al. 2007; Wang and Lee 2008]. Baran *et al.*[2007] construct a discretized geometric graph and then minimize a penalty function to penalize differences in the embedded skeleton from the given skeleton. The advantage of volumetric methods is that since they resample the object, they are insensitive to poorly shaped triangles in the initial mesh. However, they are limited by the discretization and may lack precision, especially when the mesh has thin features.

Continuous surface methods work on a polygonal mesh directly. Last year, [Au et al. 2008] proposed a simple skeleton extraction method based on Laplacian smoothing and mesh contraction. However, since it relies on a differential operator on the mesh, it fails to give good results for meshes with bad quality or with unwanted shape features like spikes, hair or fur. Methods based on Reeb graph [Aujay et al. 2007] encounter the same problem. More importantly, they cannot extract a continuous skeleton from a mesh with multiple connected components. Methods that extract the skeleton from a segmentation of the model [Katz and Tal 2003], [Schaefer and Yuksel 2007],[de Aguiar et al. 2008] suffer from the same limitation.

In this paper, we propose a volumetric method that directly uses the initial representation of the surface. At each iteration, the interior of the surface is represented by a set of tetrahedra. Therefore our approach shares the advantage of volumetric methods (robustness) and the advantage of surfacic ones (accuracy).

3 Centroidal Voronoi Tessellation for line segments and graphs

We now present our approach to generalize Centroidal Voronoi Tesselation (CVT) to line segments and graphs. Such a generalization of CVT to line segments is likely to have several applications, such as skeleton fitting and segmentation demonstrated here, and also vector field visualization or image stylization. The idea is illustrated in Figure 2. This section is illustrated with 2D examples, but note that the notions presented here are dimension independent. Our results in 3D are shown further in the paper. As shown in Figure 2, starting from an initial configuration of the skeleton, we minimize in each Voronoi cell (colors) the integral of the squared distance to the skeleton (generalized Lloyd energy). This naturally fits the edges of the skeleton into the protrusions of the mesh.

We first recall the usual definition of CVT for points (Section 3.1), then we extend the definition to line segments and graphs (Section 3.2), and introduce the approximation that we are using (Section 3.3). Section 3.4 introduces the regularization term, and Section 4 our solution mechanism.

3.1 CVT for points

CVT has diverse applications in computational science and engineering, including geometry processing [Du et al. 1999; Alliez et al. 2005] and has gained much attention in recent years. In this paper we extend the definition of CVT to make it applicable for sets of inter-connected line segments (or graphs). We first give the usual definition of Voronoi Diagram and Centroidal Voronoi Tesselation.

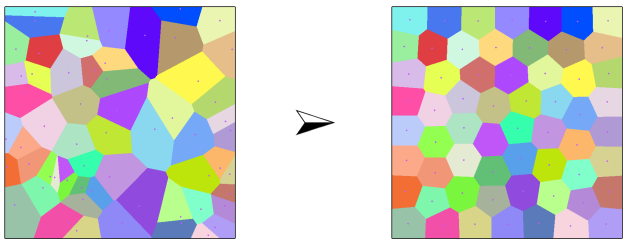

Figure 3: CVT for points in $2D$.

Let $\mathbf{X} = (\mathbf{x}_i)_{i=1}^n$ be an ordered set of n seeds in $\mathbb{R}^N$. The Voronoi region $Vor(\mathbf{x}_i)$ of $\mathbf{x}_i$ is defined by :

$$Vor(\mathbf{x}_i) = \{\mathbf{x} \in \mathbb{R}^N \mid \|\mathbf{x} - \mathbf{x}_i\| \leq \|\mathbf{x} - \mathbf{x}_j\|, \forall j \neq i\}.$$

The Voronoi regions of all the seeds form the Voronoi diagram (VD) of $\mathbf{X}$. Let us now consider a compact region $\Omega \subset \mathbb{R}^N$ (for instance, the interior of the square around Figure 3-left). The clipped Voronoi diagram is defined to be the set of clipped Voronoi cells $\{Vor(\mathbf{x}_i) \cap \Omega\}$.

A Voronoi Diagram is said to be a Centroidal Voronoi Tesselation (CVT) if each seed $\mathbf{x}_i$ coincides with the barycenter of its clipped Voronoi cell (geometric characterization). An example of CVT is shown in Figure 3-right. This definition leads to Lloyd's relaxation [Lloyd 1982], that iteratively moves all the seeds to the barycenter of their Voronoi cells. Alternatively, CVT can be also characterized in a variational way [Du et al. 1999], as the minimizer of Lloyd's energy F :

$$F(\mathbf{X}) = \sum_{i=1}^{n} f(\mathbf{x}_i) \quad ; \quad f(\mathbf{x}_i) = \int_{Vor(\mathbf{x}_i)\cap\Omega} \|\mathbf{x}-\mathbf{x}_i\|^2 \, \mathrm{d}\mathbf{x} \quad (1)$$

Using this latter variational formulation, a possible way of computing a CVT from an arbitrary configuration consists in minimizing F [Liu et al. 2008]. Now we explain how this variational point of view leads to a more natural generalization to line segments as compared to the geometric characterization used in Lloyd's relaxation.

3.2 CVT for line segments and graphs

Besides points, it is well known that general objects such as line segments can also be taken as the generators of Voronoi diagrams (see Figure 4). For instance, Hiller *et al.* [2003] have used line segments Voronoi diagrams to generalize the notion of stippling used in Non-Photorealistic Rendering. Their method uses a discretization on a pixel grid, and a heuristic based on a variant of Lloyd's relaxation to move the segments. They translate each segment to the centroid of its Voronoi cell, and then align it with the cell's inertia tensor.

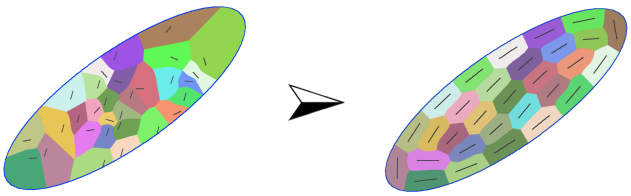

Figure 4: CVT for segments in an ellipse.

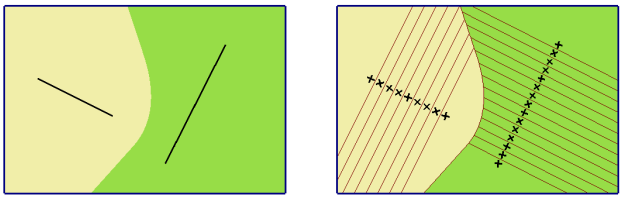

(a) (b)

Figure 5: Voronoi diagram of two line segments.(a)Accurate VD; (b)approximated VD.

In our case, it is unclear how to apply this method to a set of segments that share vertices (i.e. a graph). Moreover, using a pixel grid is prohibitively costly in 3D.

For these two reasons, we consider the variational characterization of CVT, that we generalize to line segments. Let E be the set of line segments with the end points in $\mathbf{X}$. We define the CVT energy for segment $[\mathbf{x}_i, \mathbf{x}_j]$ in Ω as:

$$g([\mathbf{x}_i, \mathbf{x}_j]) = \int_{Vor([\mathbf{x}_i,\mathbf{x}_j]) \bigcap \Omega} d(\mathbf{z}, [\mathbf{x}_i, \mathbf{x}_j])^2 \, \mathrm{d}\mathbf{z}, \quad (2)$$

where $Vor([\mathbf{x}_i, \mathbf{x}_j]) = \{\mathbf{z} \in \mathbb{R}^N \mid d(\mathbf{z}, [\mathbf{x}_i, \mathbf{x}_j]) \leq d(\mathbf{z}, [\mathbf{x}_k, \mathbf{x}_l]), \forall k, l \in E\}$ and $d(\mathbf{z}, [\mathbf{x}_i, \mathbf{x}_j])$ denotes the Euclidean distance from a point to the segment.

Particularly, when the same vertex is shared by several line segments, they define a graph. We denote this graph by $\mathcal{G} := (\mathbf{X}, E)$.

Definition 1 *A CVT for a graph $\mathcal{G} = (\mathbf{X}, E)$ is the minimizer $\mathbf{X}$ of the objective function G defined by :*

$$G(\mathbf{X}) = \sum_{i,j \in E} g([\mathbf{x}_i, \mathbf{x}_j]). \quad (3)$$

In practice, minimizing G is non-trivial, due to the following two difficulties :

- Computing the VD of line segments is complicated, since the bisector of two segments are curves (resp. surfaces in 3D) of degree 2. Some readily available software solve the $2D$ case (e.g., VRONI [Held 2001] and CGAL), but the problem is still open in $3D$;
- supposing the VD of line segments is known, integrating distances over cells bounded by quadrics is non-trivial.

3.3 Approximated CVT for segments and graphs

For these two reasons, we use an approximation. As shown in Figure 5, we replace the segment $[\mathbf{x}_i, \mathbf{x}_j]$ with a set of samples $(\mathbf{p}_k)$:

$$\mathbf{p}_k = \lambda_k \mathbf{x}_i + (1 - \lambda_k)\mathbf{x}_j \quad , \quad \lambda_k = [0, 1].$$

Then the Voronoi cell of the segment can be approximated by the union of all intermediary points' Voronoi cells, and its energy g can be approximated as follows :

$$Vor([\mathbf{x}_i, \mathbf{x}_j]) \simeq \bigcup_k Vor(\mathbf{p}_k) \quad ; \quad g([\mathbf{x}_i, \mathbf{x}_j]) \simeq \sum_k f(\mathbf{p}_k)$$

where f denotes the point-based energy (Equation 1).

This yields the following definition :

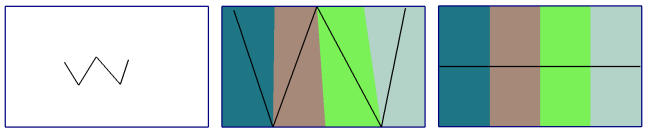

(a) (b) (c)

Figure 6: A chained graph with 5 vertices and 4 edges.(a)Input; (b)minimizer of CVT energy; (c)with regularization energy $\gamma = 0.01$.

Definition 2 *An Approximate CVT for a graph* $\mathcal{G} = (\mathbf{X}, E)$ *is the minimizer* $\mathbf{X}$ *of the objective function* $\widetilde{G}$ *defined by :*

$$\widetilde{G}(\mathbf{X}) = \sum_{i,j \in E} \sum_{k} f(\mathbf{p}_k) = \sum_{i,j \in E} \sum_{k} f(\lambda_k \mathbf{x}_i + (1-\lambda_k)\mathbf{x}_j). \tag{4}$$

where f *denotes the point-based energy (Equation 1).*

Since it is based on a standard Voronoi diagram and Lloyd energy, the so-defined approximated objective function $\widetilde{G}$ is much simpler to optimize than the original G given in Equation 3. Note that G and $\widetilde{G}$ depend on the same variables $\mathbf{X}$. The intermediary samples $\mathbf{p}_k = \lambda_k \mathbf{x}_i + (1-\lambda_k)\mathbf{x}_j$ are not variables, since they depend linearly on $\mathbf{x}_i$ and $\mathbf{x}_j$.

To avoid degenerate minimizers, we now introduce a stiffness regularization term, similarly to what is done in variational surface design.

3.4 Regularization, stiffness

The CVT energy tends to maximize the compactness of the dual Voronoi cells, which is desired in general. However, some particular configurations may lead to unwanted oscillations. For instance, the (undesired) configuration shown in Figure 6(b) has a lower energy than the one shown in Figure 6(c). Intuitively, the long thin cells in (c) have points that are far away from the skeleton. To avoid the configuration in (b) and favor the one in (c), we add a regularization term $R(\mathbf{X})$ to the energy functional, defined as the squared graph Laplacian, that corresponds to the *stiffness* of the joints :

$$R(\mathbf{X}) = \sum_{\mathbf{x}_i, v(\mathbf{x}_i)>1} \|\mathbf{x}_i - \frac{1}{v(\mathbf{x}_i)} \sum_{\mathbf{x}_j \in N(\mathbf{x}_i)} \mathbf{x}_j\|^2, \tag{5}$$

where $v(\mathbf{x}_i)$ denotes the valence, $N(\mathbf{x}_i)$ the neighbors of $\mathbf{x}_i$.

We can now define the objective function $\mathcal{F}$ minimized by our approach :

$$\mathcal{F}(\mathbf{X}) = \widetilde{G}(\mathbf{X}) + \gamma |\Omega| R(\mathbf{X}). \tag{6}$$

where $\widetilde{G}(\mathbf{X})$ is the approximated Lloyd energy of the segments (Equation 4) and $R(\mathbf{X})$ is the regularization term (Equation 5). $\gamma \in \mathbb{R}^+$ denotes the influence of the regularization term. We used $\gamma = 0.01$ in all our experiments. Note that the regularization term R is multiplied by the volume of the object $|\Omega|$ so that $\widetilde{G}$ and R have compatible dimensions.

Figure 7 shows the influence of the parameter γ. For valence 2 nodes, a high value of γ tends to straighten the joints. For branching nodes, a high value of γ tends to homogenize the segment angles and lengths. In our experiments, good results were obtained with $\gamma = 0.02$. It is also possible to assign a different stiffness γ_i to each joint, to improve joint placement, but since this introduces too many parameters, we will show later a simpler method to automatically optimize joint placements, without needing any additional parameter.

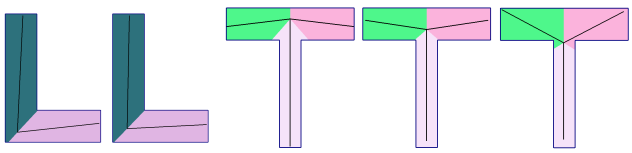

(a) (b)

Figure 7: (a)$\gamma = 0, 0.01$ from left to right; (b) $\gamma = 0, 0.03, 0.1$ respectively from left to right.

4 Solution mechanism

To minimize the objective function $\mathcal{F}$, we use an efficient quasi-Newton solver. A recent work on the CVT energy showed its C^2 smoothness [Liu et al. 2008] (except for some seldom encountered degenerate configurations where it is C^1). In our objective function $\mathcal{F}$, the term $\tilde{G}$ composes linear interpolation with the Lloyd energy, and the regularization term R is a quadratic form. Therefore, $\mathcal{F}$ is also of class C^2, which allows us to use second-order optimization methods. As such, Newton's algorithm for minimizing functions operates as follows :

(1) while $\|\nabla\mathcal{F}(\mathbf{X})\| > \epsilon$
(2) solve for $\mathbf{d}$ in $\nabla^2\mathcal{F}(\mathbf{X})\mathbf{d} = -\nabla\mathcal{F}(\mathbf{X})$
(3) find a step length α such that $\mathcal{F}(\mathbf{X} + \alpha\mathbf{d})$ sufficiently decreases
(4) $\mathbf{X} \leftarrow \mathbf{X} + \alpha\mathbf{d}$
(5) end while

where $\nabla\mathcal{F}(\mathbf{X})$ and $\nabla^2\mathcal{F}(\mathbf{X})$ denote the gradient of $\mathcal{F}$ and its Hessian respectively. Computing the Hessian (second-order derivatives) can be time consuming. For this reason, we use L-BFGS [Liu and Nocedal 1989], a quasi-Newton method that only needs the gradient (first-order derivatives). The L-BFGS algorithm has a similar structure, with a main loop that updates $\mathbf{X}$ based on evaluations of $\mathcal{F}$ and $\nabla\mathcal{F}$. The difference is that in the linear system of line (2), the Hessian is replaced with a simpler matrix, obtained by accumulating successive evaluations of the gradient (see [Liu and Nocedal 1989] and [Liu et al. 2008] for more details).

In practice, one can use one of the readily available implementations of L-BFGS (e.g. TAO/Petsc).

Thus, to minimize our function $\mathcal{F}$ with L-BFGS, what we need now is to be able to compute $\mathcal{F}(\mathbf{X})$ and $\nabla\mathcal{F}(\mathbf{X})$ for a series of $\mathbf{X}$ iterates, as in the following outline, detailed below (next three subsections).

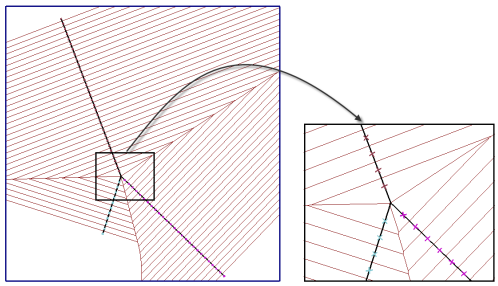

Figure 8: Illustration of the sampling on the segments.

Algorithm outline - CVT for line segments and graphs

For each Newton iterate $\mathbf{X}$

1. For each segment $[\mathbf{x}_i, \mathbf{x}_j]$, generate the samples $\mathbf{p}_k$;
2. For each $\mathbf{p}_k$, compute the clipped Voronoi cell of $\mathbf{p}_k$, i.e. $Vor(\mathbf{p}_k) \cap \Omega$ where Ω denotes the interior of the surface ;
3. Add the contribution of each $\mathbf{p}_k$ to $\mathcal{F}$ and $\nabla\mathcal{F}$.

4.1 Generate the samples $\mathbf{p}_k$

We choose a sampling interval h. In our experiments, $1/100^{th}$ of the bounding box's diagonal gives sufficient precision. We then insert a sample every h along the segments. Terminal vertices (of valence 1) are inserted as well.

Vertices $\mathbf{x}_i$ of valence greater than 1 are skipped, in order to obtain a good approximation of the bisectors near branching points (see Figure 8).

4.2 Compute the clipped Voronoi cells

We now compute the Delaunay triangulation of the samples $\mathbf{p}_k$ (one may use CGAL for instance), and then the Voronoi diagram is obtained as the dual of the Delaunay triangulation. Now we need to compute the intersections between each Voronoi cell $Vor(\mathbf{p}_k)$ and the domain Ω, defined as the interior of a triangulated surface. Since Voronoi cells are convex (and not necessarily the surface), it is easier (though equivalent) to consider that we clip the surface by the Voronoi cell. To do so, we use the classical re-entrant clipping algorithm [Sutherland and Hodgman 1974], recalled in Figure 9-A, that considers a convex window as the intersection of half-spaces applied one-by-one to the clipped object. In our 3D case, when clipping the triangulated surface with a half-space, each triangle can be considered independently. We show an example in Figure 9-B, where two bisectors generate Homer's "trousers". Since it processes the triangles one by one, the algorithm is extremely simple to implement, and does not need any combinatorial data structure. Moreover, it can be applied to a "triangle soup", provided that the polygons have correct orientations (i.e., coherent normals).

However, it is important to mention that the surface needs to be closed after each half-space clipping operation. This is done by connecting each intersection segment (thick red in Figure 9-C) with the first intersection point, thus forming a triangle fan. Note that when the intersection line is non-convex, this may generate geometrically incorrect configurations, such as the sheet of triangles between the legs

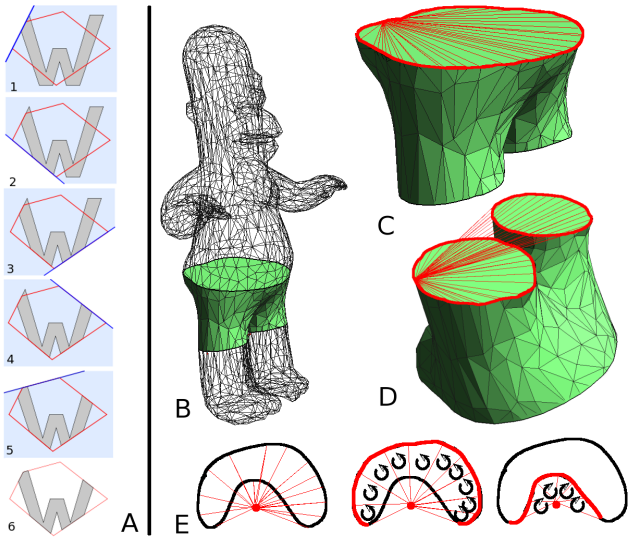

Figure 9: Sutherland-Hogdman re-entrant clipping.

in Figure 9-D. However, this configuration is correct from a computational point of view, if we keep the orientation of the triangles, as explained in Figure 9-E. Suppose we want to compute the area of the "bean" shape, by summing triangles connected to the red vertex. With the orientation of the triangles, the extraneous area appears twice, with a positive and negative orientation that cancel-out. After the clipping operation, the clipped Voronoi cell of the point $\mathbf{p}_k$ is represented by its boundary, as a list of triangles $(\mathbf{q}_i, \mathbf{q}_j, \mathbf{q}_k)$. The interior of the Voronoi cell is obtained as a set of oriented tetrahedra $(\mathbf{p}_k, \mathbf{q}_i, \mathbf{q}_j, \mathbf{q}_k)$, created by connecting $\mathbf{p}_k$ to each triangle. Note also that $\mathbf{p}_k$ may be outside its clipped Voronoi cell, but again, with the orientation of the tetrahedra, this still gives the correct result for Lloyd's energy, barycenter and mass computed in the next section.

4.3 Add the contributions to $\mathcal{F}$ and $\nabla\mathcal{F}$

We first consider the approximated segment Lloyd energy $\widetilde{G}$. The CVT energy associated with a tetrahedron $T = (\mathbf{p}_k, \mathbf{q}_1, \mathbf{q}_2, \mathbf{q}_3)$ is given by

$$\frac{|T|}{10}(\mathbf{U}_1^2 + \mathbf{U}_2^2 + \mathbf{U}_3^2 + \mathbf{U}_1.\mathbf{U}_2 + \mathbf{U}_2.\mathbf{U}_3 + \mathbf{U}_3.\mathbf{U}_1),$$

where $\mathbf{U}_i = \mathbf{q}_i - \mathbf{p}_k$ and $|T|$ denotes the oriented volume of T. To compute the gradients, we first recall the gradient of the point-based Lloyd energy [Du et al. 1999], given by :

$$\begin{aligned} &\tfrac{\partial F}{\partial \mathbf{p}_k} = 2m_k(\mathbf{p}_k - \mathbf{c}_k) \\ &\text{where:} \\ &m_k = \int_{Vor(\mathbf{p}_k)\cap\Omega} d\mathbf{x} \quad ; \quad \mathbf{c}_k = \tfrac{1}{m_k}\int_{Vor(\mathbf{p}_k)\cap\Omega} \mathbf{x}d\mathbf{x} \end{aligned} \tag{7}$$

By applying the chain rule to the expression of the intermediary points $\mathbf{p}_k = \lambda_k\mathbf{x}_i + (1-\lambda_k)\mathbf{x}_j$, we obtain the gradient

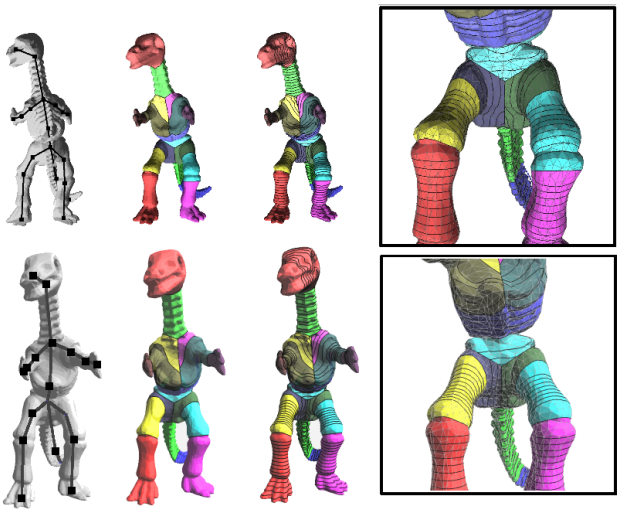

Figure 10: Fitting and segmentation before (top) and after joint optimization (bottom). Notice the rightmost knee.

of $\widetilde{G}$ for the edge $[\mathbf{x}_i, \mathbf{x}_j]$:

$$\begin{aligned}
\frac{\partial \widetilde{G}}{\partial \mathbf{x}_i} &= \sum_k \frac{\partial f(\mathbf{p}_k)}{\partial \mathbf{x}_i} \\
&= \sum_k \frac{\partial f(\mathbf{p}_k)}{\partial \mathbf{p}_k} \frac{\partial \mathbf{p}_k}{\partial \mathbf{x}_i} = 2 \sum_k m_k (\mathbf{p}_k - \mathbf{c}_k) \lambda_k; \\
\frac{\partial \widetilde{G}}{\partial \mathbf{x}_j} &= \sum_k \frac{\partial f(\mathbf{p}_k)}{\partial \mathbf{x}_j} = 2 \sum_k m_k (\mathbf{p}_k - \mathbf{c}_k)(1 - \lambda_k),
\end{aligned}$$

where m_k and $\mathbf{c}_k$ denote the mass and the centroid of $Vor(\mathbf{p}_k) \cap \Omega$ respectively (see Equation 7). Note that m_k and $\mathbf{c}_k$ can be easily computed from the clipped Voronoi cell, represented by a union of oriented tetrahedra (see section 4).

The gradient of $\widetilde{G}$ with respect to the graph vertex $\mathbf{x}_i$ gathers the contributions of all the gradients of the sampling points $\mathbf{p}_k$ in the segments incident to $\mathbf{x}_i$.

The contribution of the regularization term to the gradient ∇R is given by :

$$\frac{\partial R}{\partial \mathbf{x}_i} = 2|\Omega|\gamma_i \left(\mathbf{x}_i - \frac{1}{v(\mathbf{x}_i)} \sum_{\mathbf{x}_j \in N(\mathbf{x}_i)} \mathbf{x}_j \right).$$

4.4 Optimize joint placement

The objective function F only takes geometry into account, and does not necessarily places the joints where the user expects them. For instance, for a straight arm, the joint will be located at the middle, which does not necessarily corresponds to the elbow. However, from the information computed by our algorithm, it is easy to optimize the location of the joints. Our algorithm computes all the intersections between the Voronoi cells and the mesh, shown as black lines in Figure 10. Each black line is associated with a sample of the skeleton. The elbows correspond to constrictions, i.e. black lines of minimal length. Therefore, for each joint, we determine the sample in the neighborhood of the joint that has an intersection curve of minimal length, and move the joint to the location of this sample. For each joint $\mathbf{x}_i$, we test the samples in all the bones connected to $\mathbf{x}_i$, in the half of the bone that contains $\mathbf{x}_i$.

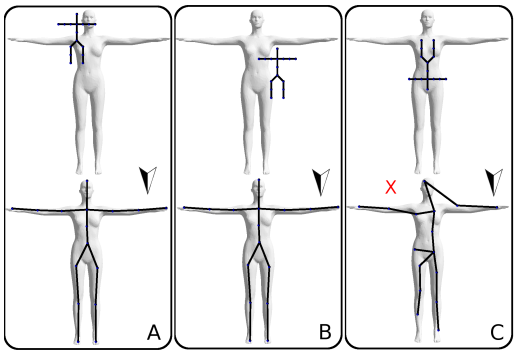

Figure 11: Influence of the initialization.

5 Results and conclusion

We have experimented with our method using several datasets. For a typical mesh, our method converged in 5 Newton iterations, which takes 2 minutes on a 2.5 GHz machine.

As demonstrated in Figure 11, our method is reasonably independent of the initial position (A,B), but may fail for more extreme initially mismatched configurations (C). In subsequent tests, initialization is provided by aligning the bounding box of the skeleton, as done in [Baran and Popović 2007]. Our method is robust to mesh degeneracies (Figure 12), such as T-Junctions, and small gaps (red lines), thanks to the accurate computation of clipped Voronoi cells (thick black lines) and the triangle-by-triangle (or tet-by-tet) integration. Figure 13 shows that noisy meshes with skinny triangles can be processed without any numerical instability (data acquired by the Visual Hull technique). To our knowledge, this is the first method that achieves this degree of robustness.

Figure 14 shows the influence of the edge sampling interval h, used to approximate the segment Voronoi cells. As can be seen, a coarse sampling is sufficient to obtain a result similar to the one obtained with a finer sampling. However, we use $h = 1/100^{th}$ of the bounding box diagonal (left), to have enough samples for the joint placement optimization phase (Section 4.4).

We show in Figure 15 some examples from the SHREK database. More examples are shown in Figure 16. Except for a small number of failure cases (red crosses), satisfying results were obtained. Our method was successfully applied to meshes with degeneracies (multiple components, holes, T-junctions) that cannot be processed by previous work. In addition, a segmentation is obtained, that can be used for matching features between meshes and morphing. Our method failed in some cases. One example of failure is shown in Figure 15 (red cross), where the arms are close to the body.

Figure 17 compares our method with the method using mesh contraction [Au et al. 2008]. The Monkey's hair appear as singularities in Laplacian computation (A). Our volumetric method is not affected by these singularities (B). Surfacic methods cannot generate a connected skeleton for a mesh with multiple components (C), whereas our volumetric approach does not "see" the boundaries between them (D).

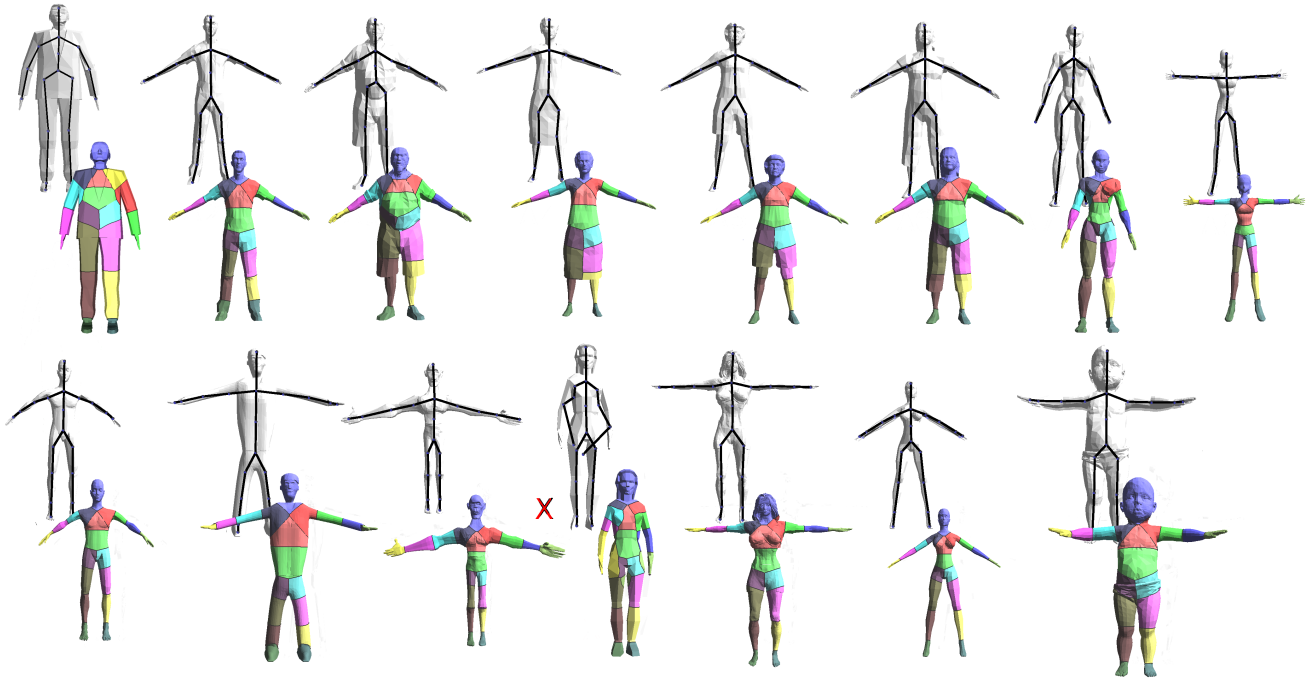

Figure 15: Humen from the SHREK database.

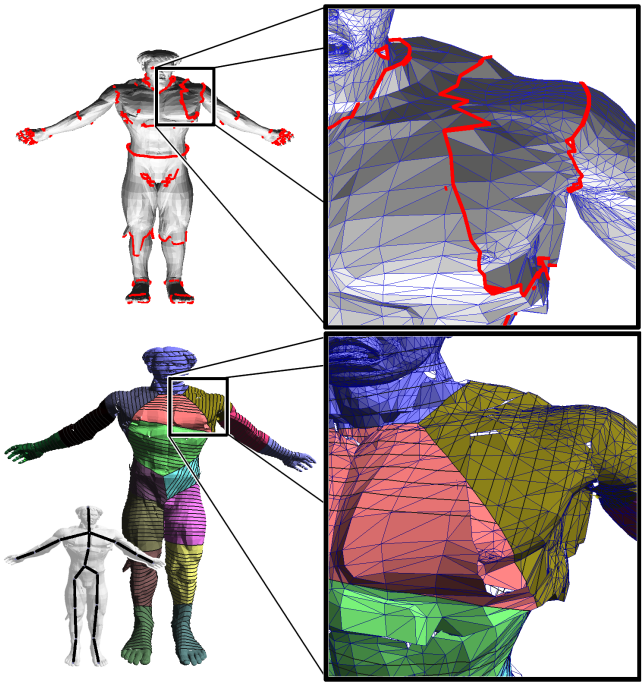

Figure 12: Robustness to mesh degeneracies (small holes).

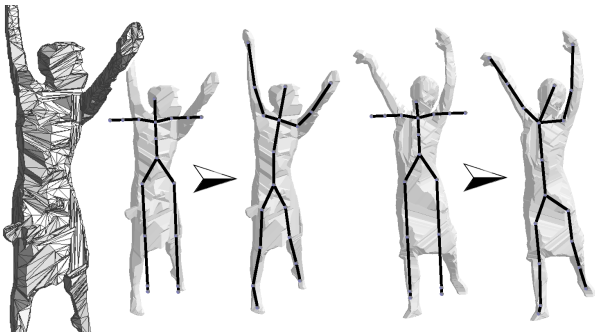

Figure 13: Robustness to mesh degeneracies (flat triangles).

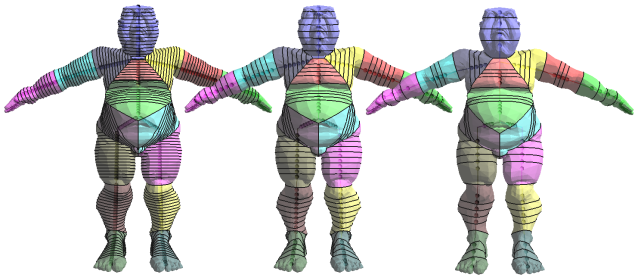

Figure 14: Influence of the skeleton sampling. With a coarse sampling of the skeleton (right) one obtains a result similar to the one obtained with a finer sampling (left).

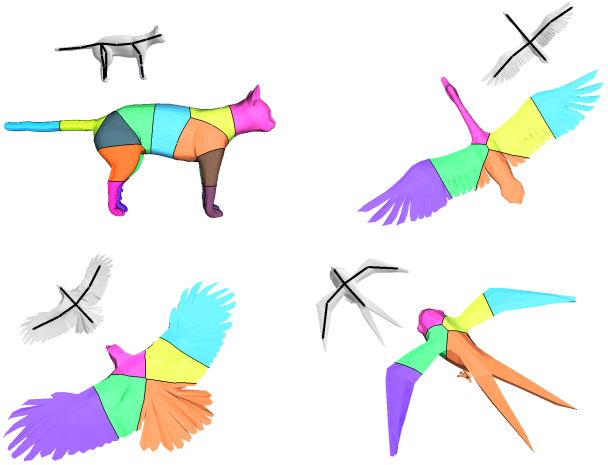

Figure 16: More results of our method.

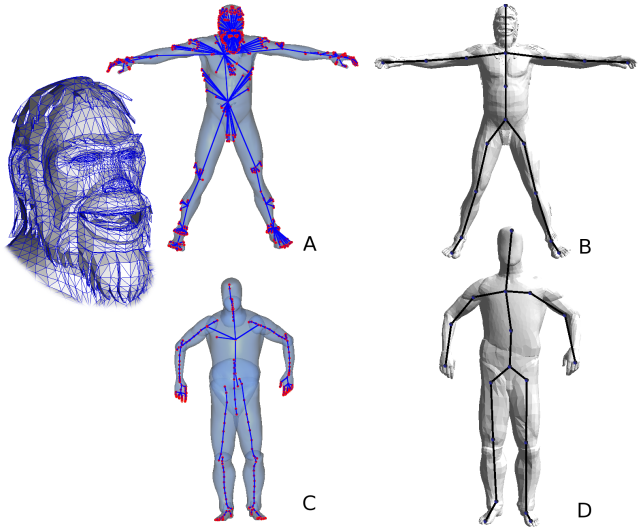

Figure 17: Comparison between Au *et al.*'s mesh-contraction (left) and our method (right).

Conclusion We have presented in this paper a new method for variational skeleton fitting. Its main advantages are :

- **Simplicity**: the problem of skeleton fitting is expressed in variational form (Equation 6), requiring no more than minimizing an objective function. The gradients are easily computed by our Voronoi clipping;
- **Robustness**: the triangle-by-triangle integration (tet-by-tet) does not need a connected mesh, and does not estimate differential quantities, therefore our method works with degenerate meshes.

This paper showed results for skeleton fitting and shape segmentation. We think that other applications are possible, such as shape morphing, shape retrieval and markerless motion capture by fitting skeletons to mesh sequences acquired by computer vision. We showed that generalizing the Centroidal Voronoi Tesselation framework to primitives that are more general than points is possible. Beyond the graph of segments considered here, in future work we will consider CVT-based shape optimization by defining CVT with other types of primitives (i.e. cylinders, plates . . .).

Acknowledgments will be given in the final version.

References

Alliez, P., Meyer, M., and Desbrun, M. 2002. Interactive Geometry Remeshing. *ACM TOG (Proc. SIGGRAPH) 21(3)*, 347–354.

Alliez, P., Cohen-Steiner, D., Yvinec, M., and Desbrun, M. 2005. Variational tetrahedral meshing. *ACM TOG (Proc. SIGGRAPH)*.

Au, O. K.-C., Tai, C.-L., Chu, H.-K., Cohen-Or, D., and Lee, T.-Y. 2008. Skeleton extraction by mesh contraction. *ACM TOG (Proc. SIGGRAPH*.

Aujay, G., Hétroy, F., Lazarus, F., and Depraz, C. 2007. Harmonic skeleton for realistic character animation. In *Proc. SCA*.

Baran, I., and Popović, J. 2007. Automatic rigging and animation of 3d characters. *ACM TOG (Proc. SIGGRAPH*.

Cohen-Steiner, D., Alliez, P., and Desbrun, M. 2004. Variational shape approximation. *ACM TOG (Proc. SIGGRAPH)*.

Cornea, N. D., and Min, P. 2007. Curve-skeleton properties, applications, and algorithms. *IEEE TVCG 13*, 3.

de Aguiar, E., Theobalt, C., Thrun, S., and Seidel, H.-P. 2008. Automatic Conversion of Mesh Animations into Skeleton-based Animations. *Computer Graphics Forum (Proc. Eurographics)*.

Du, Q., Faber, V., and Gunzburger, M. 1999. Centroidal Voronoi tessellations: applications and algorithms. *SIAM Review*.

Held, M. 2001. VRONI: An engineering approach to the reliable and efficient computation of voronoi diagrams of points and line segments. *Computational Geometry: Theory and Applications*.

Hiller, S., Hellwig, H., and Deussen, O. 2003. Beyond stippling-methods for distributing objects on the plane. *Computer Graphics Forum*.

Ju, T., Baker, M. L., and Chiu, W. 2007. Computing a family of skeletons of volumetric models for shape description. *CAD*.

Katz, S., and Tal, A. 2003. Hierarchical mesh decomposition using fuzzy clustering and cuts. *ACM TOG*.

Liu, D. C., and Nocedal, J. 1989. On the limited memory BFGS method for large scale optimization. *Mathematical Programming: Series A and B 45*, 3, 503–528.

Liu, Y., Wang, W., Lévy, B., Sun, F., Yan, D. M., Lu, L., and Yang, C. 2008. On centroidal voronoi tessellation - energy smoothness and fast compu tation. Tech. rep., Hong-Kong University and INRIA - ALICE Project Team. Accepted pending revisions.

Lloyd, S. P. 1982. Least squares quantization in PCM. *IEEE Transactions on Information Theory 28*, 2, 129–137.

Schaefer, S., and Yuksel, C. 2007. Example-based skeleton extraction. In *Proc. SGP*.

Sutherland, I. E., and Hodgman, G. W. 1974. Reentrant polygon clipping. *Comm. ACM 17*, 1, 32–42.

Valette, S., and Chassery, J.-M. 2004. Approximated centroidal Voronoi diagrams for uniform polygonal mesh coarsening. *Computer Graphics Forum (Proc. Eurographics)*.

Valette, S., Chassery, J.-M., and Prost, R. 2008. Generic remeshing of 3D triangular meshes with metric-dependent discrete Voronoi diagrams. *IEEE TVCG*.

Wang, Y.-S., and Lee, T.-Y. 2008. Curve-skeleton extraction using iterative least squares optimization. *IEEE TVCG*.